Supplementary information

Morphological changes of silica aged in environmental conditions by three-dimensional nano-scale quantifications

Bruno Chal[1], Lucian Roiban[1], Guilhem P. Baeza[1], Karine Masenelli-Varlot[1],

Jacques Jestin[2], Bernard Yrieix[3] and Geneviève Foray[1,*]

* Corresponding author: genevieve.foray@insa-lyon.fr, +33 4 72 43 61 28

[1] Univ Lyon, INSA Lyon, UCBL, CNRS, MATEIS, UMR 5510, 7 avenue Jean Capelle, F-69621, Villeurbanne, France

[2] CEA, LLB, CEA Saclay, GIF SUR YVETTE CEDEX - ST AUBIN, F-91191 , France

[3] EDF R&D, Les Renardières, MORET SUR LOING, F-77250 , France

BF TEM images of unaged silica, and silica aged for 24 days and 96 days at 70°C and 90% relative humidity (RH).

There after we present different spatial resolution images as well as the particle size distribution in the case of:

- Unaged silica (Fig SI1)
- Silica aged for 24 days at 70°C and 90% RH (Fig SI2)
- Silica aged for 96 days at 70°C and 90% RH (Fig SI3)

The particle size distributions were obtained by considering the projected surface as the surface of an equivalent disc. The small black dots are gold nanoparticles used to align the electron tomography acquisitions. Here it must be mentioned that the analysis by electron microscopy was made on the native dispersed powder. In particular, no compression was applied during sample preparation.

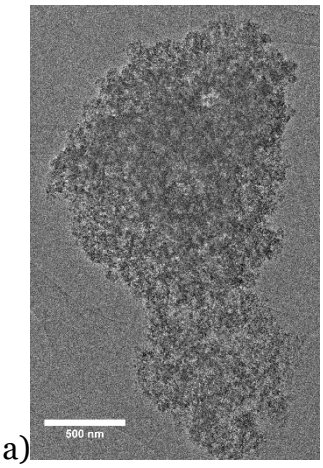

a)

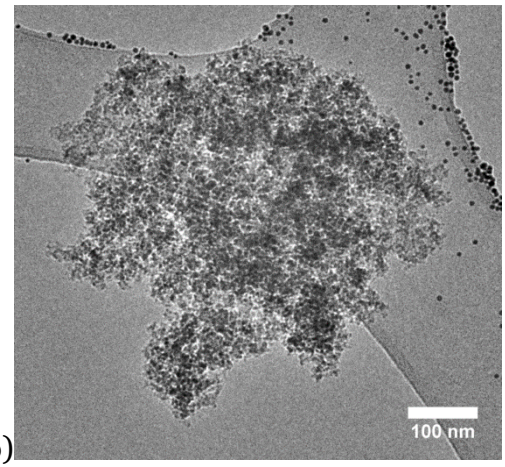

b)

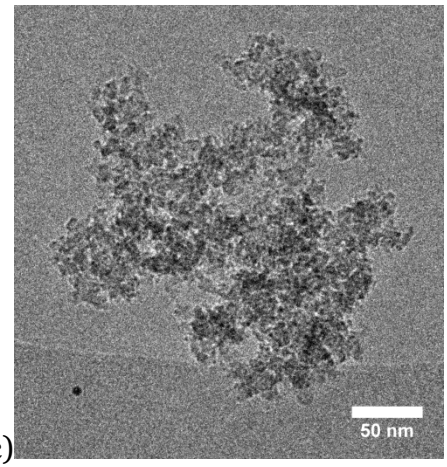

c)

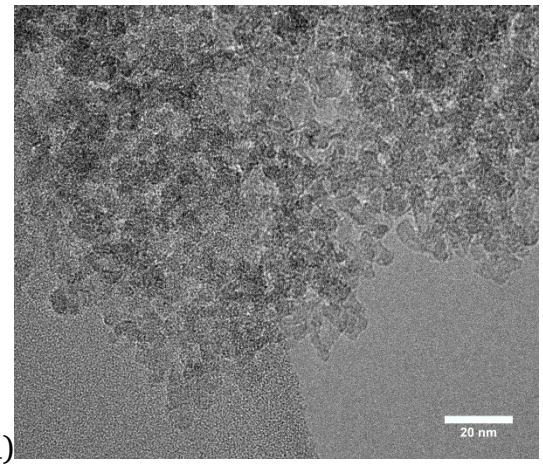

d)

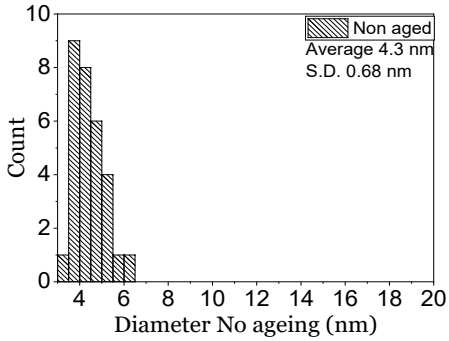

e)

Fig SI1: 2D TEM analysis of unaged silica. The TEM micrographs (a-d) show that the non-aged silica is formed by individual grains form aggregates and then form agglomerates. The dispersed powder micrographs were acquired at different spatial resolutions in order to have a wide field of view and to highlight the material ultraporous structure. The particle size distribution (e) was computed from the images (2D projections). The diameter of the smallest circle including the particle was measured. At the initial stage, the particles have relatively regular shapes assimilated to a projected oval. The average particle diameter is 4.3 nm, with a standard deviation of 0.68 nm.

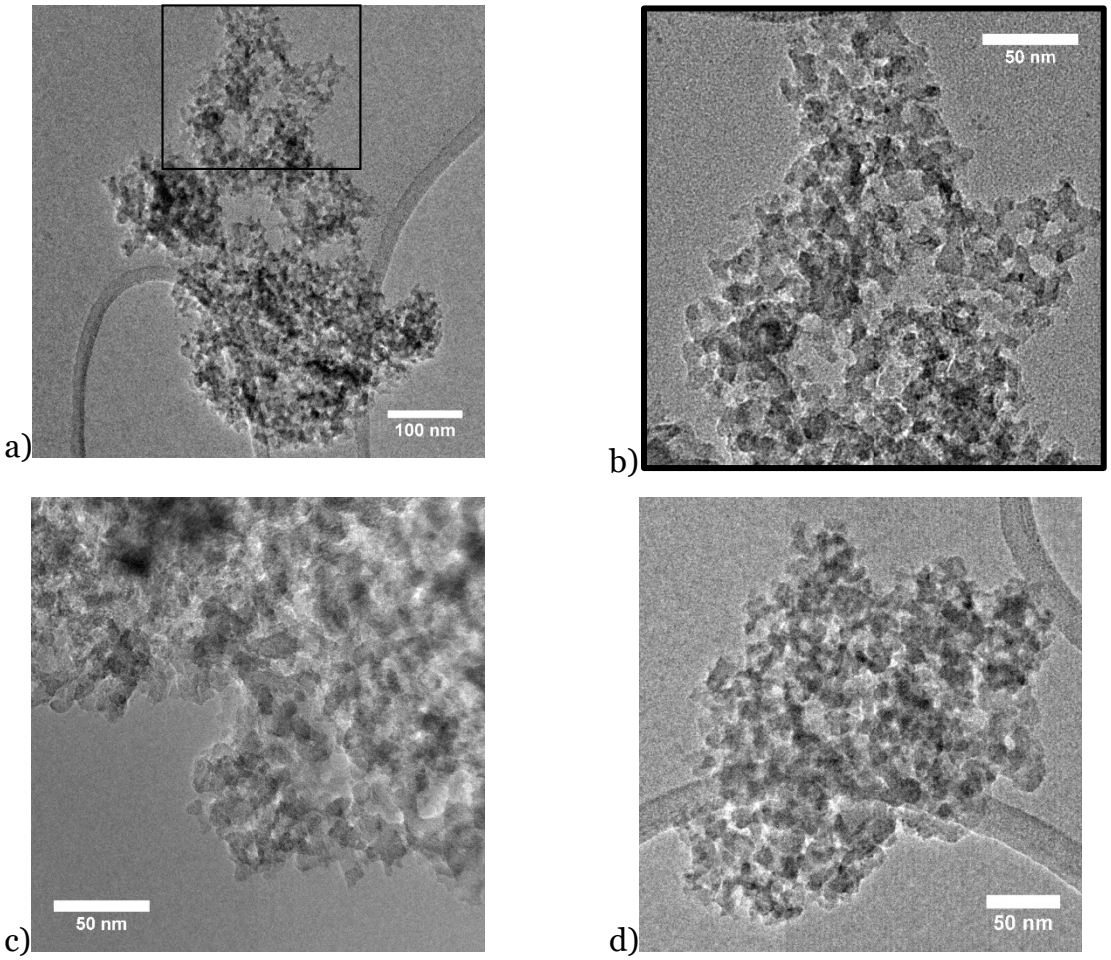

Fig SI2: 2D TEM analysis of silica aged for 24 days at 70°C and 90% RH. TEM micrographs (a-d) show a coarser structure. The location of micrograph b) is indicated by the black rectangle in image a). After a short ageing (24 days) the average particle size increases from 4.3 nm up to 7.0 nm as shown by the particle size distribution (e). Please note that the standard deviation increases too. As highlighted in micrograph b), the cross open pore size increases and some are now larger than 30 nm. Such pores are delimited by 'walls' made of particles. Those walls become uniform as ageing proceeds and particles are fused.

a)

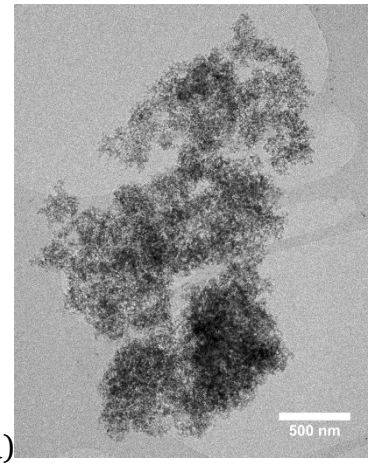

b)

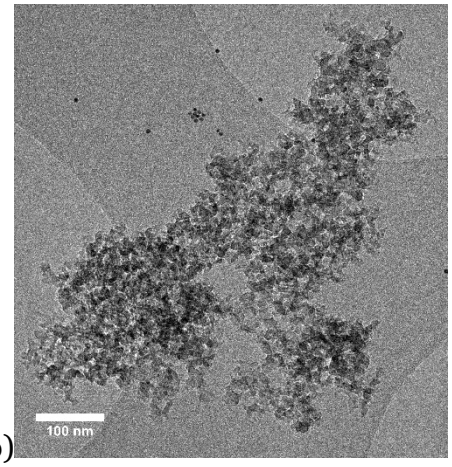

c)

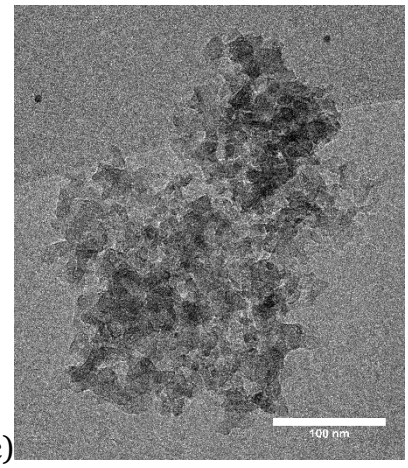

d)

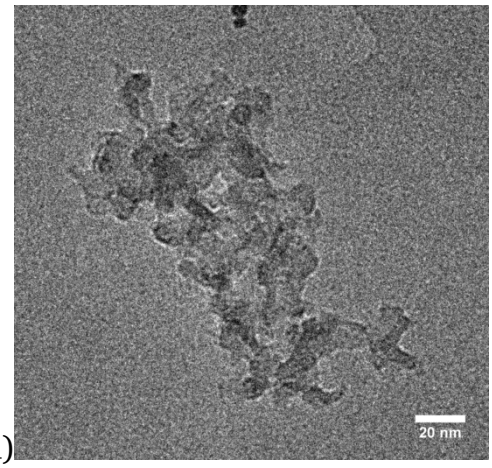

e)

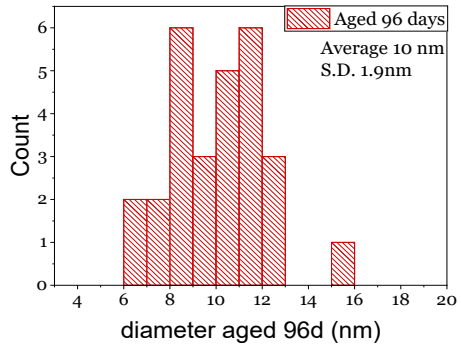

Fig SI3: **2D** TEM analysis of silica aged for 96 days at 70°C and 90% RH. TEM micrographs are shown in a-d. The particle size distribution is represented in e. After a long ageing (96 days) the average particle size (e) increases from 4.3 nm up to 10.0 nm (see also in the images (a-d). Please note that the standard deviation keeps increasing, with particles now as large as 16 nm. Micrograph d) reveals that the particles have less regular shapes – initial no ageing oval shape are scarce. By becoming larger, the particles are forming aggregates including larger cross pores new building blocks.

BET

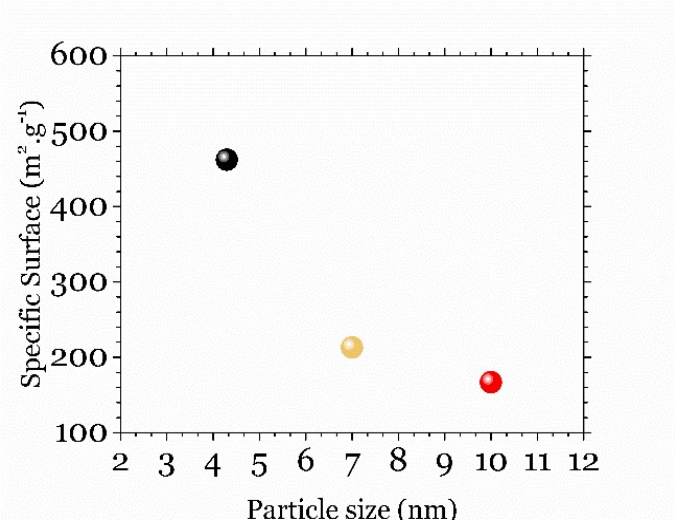

Fig SI4: Specific surface area determined with a BET method from nitrogen sorption measurements (black, no ageing. other colors aged at 70 °C under 90%RH for 24 days and 96 days respectively) as a function of the mean particle size determined by **2D** TEM. The specific surface area decreases as the mean particle size increases.

Step-by-step electron tomography at low dose

Electron tomography was performed by using an improved method based on step-by-step fast image acquisition[1]. . Such method is based on the acquisition of bright-field tilted images. It was chosen because of the high beam-sensitivity of the samples. Indeed, it is possible to record tilt series in 5-7 seconds with a low electron dose. Moreover, in the present study, the samples are all composed of amorphous silica and do not give rise to diffraction contrast.

Electron tomography was performed only on the non-aged and on the sample aged during 96 days at 70°C and 90% RH. The holey carbon grid supporting the dispersed silica powder offered hundreds of objects lying on the grid. Among them, a few ones were selected to acquire tomography acquisition series. The tilt series were composed by 75 4k*4k images, a pixel representing 0.2 nm. The acquisition time for one tilt series was equal to 138 s.

Silica is a very beam sensitive sample that degrades drastically at a relatively low electron dose[1]. It was then necessary to measure and control the electron dose received by the sample during the tilt series acquisition. The tilt series of the non-aged sample was recorded at an electron dose rate of 12.5 e^-/A^2 s. The total electron dose received by the sample during the whole acquisition was calculated to be equal to 1716 e^-/A^2. For the aged silica sample, the electron dose rate and the total electron dose received by the sample were equal to 17.8 e^-/A^2s and 2464 e^-/A^2, respectively.

Fig SI5 shows 3 2D projections of the non-aged silica that are extracted from the 75 images tilt series used to reconstruct the volume. Due to the very low dose rate, the

contrast in the recorded images is poor. Nevertheless, the observed object has a non-regular morphology, as found by using TEM analysis (see Fig SI1).

Slices extracted from the reconstructed volumes are given in Fig SI6. To facilitate the comparative analysis, the non-aged material is shown on the left and the aged material on the right. Fig SI6 a-c give XY slices through the same object volume of the non-aged silica, at different depths. Fig SI6 d-f give slices through a unique aged silica object, at different depths. It can be noticed that the contrast between the vacuum and the silica particles increases. Particle edges and pore roughness are thus better defined. In aged silica, some aggregates show internal closed pores. Fig 6g shows a 3nm closed pore (from left to right, 3 different slices at z = 0 nm, z = -1.6 nm and z = -4 nm). The size of this pore is significantly above the spatial resolution. Moreover, such pores were not present in non-aged silica. The cross-sections represented in Fig SI7 confirm such modifications. Key features are identified and their dimensions are given in Fig SI7.

The corresponding reconstructed volumes are composed of 2001 and 1910 slices for non-aged and aged silica, respectively. Several movies are available as SI:

- reconstructed volume non-aged silica. For upload, the volume was rescaled.
- reconstructed volume for silica aged for 96 days at 70 °C and 90%RH. Please refer to online version available on CLYM channel: (https://www.youtube.com/watch?v=1IhopVjBtBk) For upload, the volume was rescaled.
- closed pore inside the silica net, closure is due to ageing for 96 days at 70 °C under 90 %RH. The movie is extracted from the reconstructed volume presented above. For upload, the volume was rescaled. Online version available on CLYM channel: https://www.youtube.com/watch?v=xcIVvd-d1qA
- 3D model for aged silica obtained by segmentation of the reconstructed volume after ageing for 96 days at 70 °C under 90%RH.

From the movies, the entangled porous network of the non-aged silica is not organized, highly tortuous. Particles and pores exhibit about the same size. Particles are linked to their neighbors by necks. Posts of a few particles length or thickness are noticed. Object edges form hanging arms or smooth shallow hills. As ageing proceeds, some compact aggregates form, the roughness of pore walls decreases, small pores are dismissed, pores get larger. Neighbor particles merge and fuse as ageing time increases. Few closed pores are observed (those were formerly open and lied between initial non aged particles).

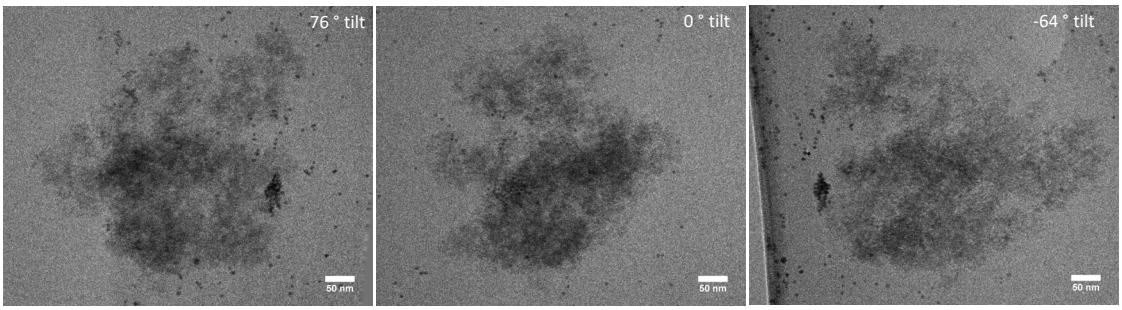

Fig SI5: 2D projections of the non-aged silica extracted from the acquired tilt series, with tilt angles equal to 76°, 0° and -64°.

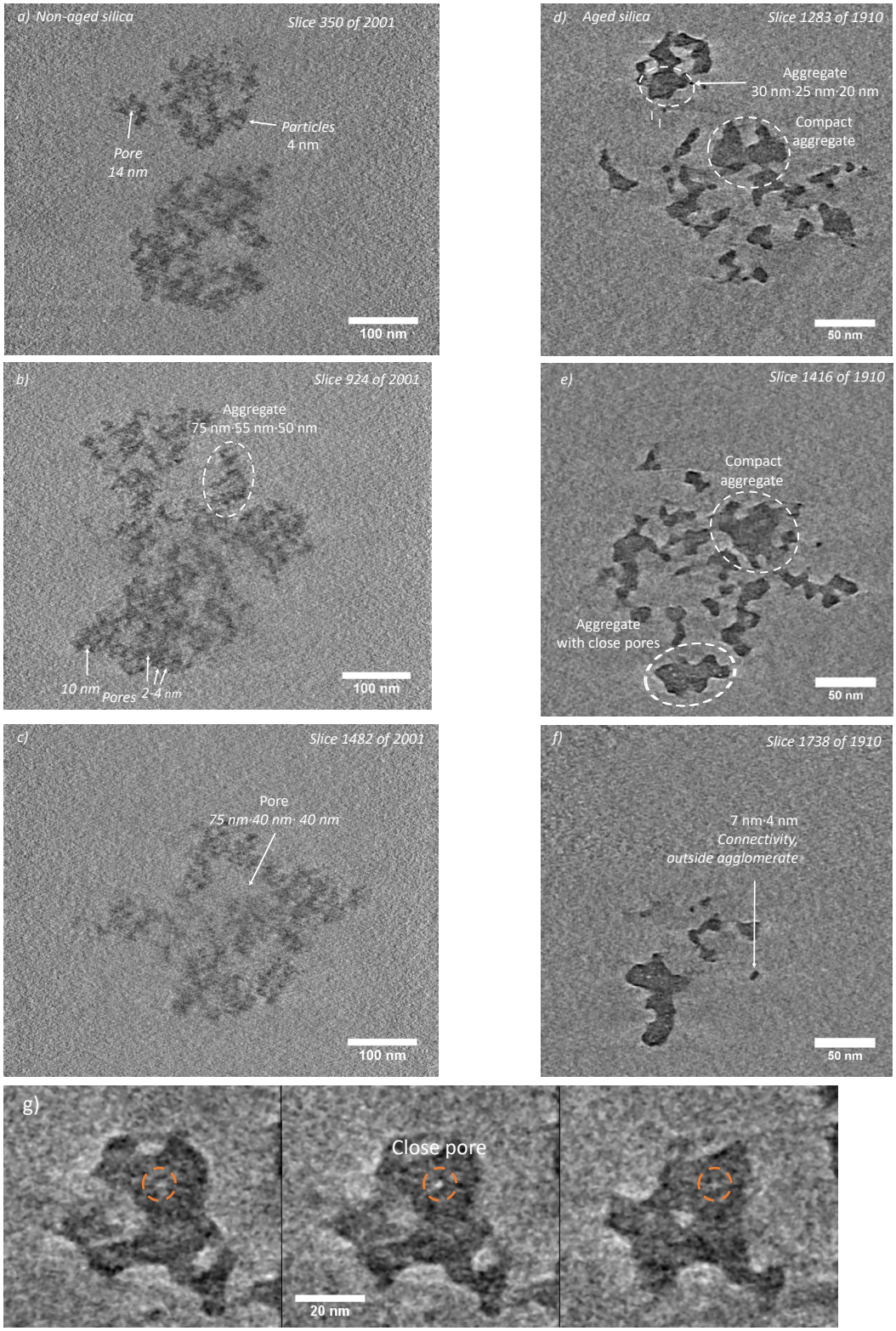

Fig SI6: Step-by-step low dose electron tomography; XY Cross-sections of the reconstructed volume. a) b) and c) non–aged silica (film of the volume available) d) e) and f) silica aged for 96 days at 70 °C under 90%RH (film of the volume available). Pores are in lighter gray and silica in darker gray. Non-aged silica has a very complex isotropic pores network formed between the silica particles. In aged silica, the silica particles coalesce, and form denser aggregates at larger scale. The pores become larger and their anisotropy increases. Some closed pores are now observed as shown in g) where a 3 nm specimen is circled (film available). The aggregate sizes reported in b) and d) were made by taking the three largest object dimensions along orthogonal directions.

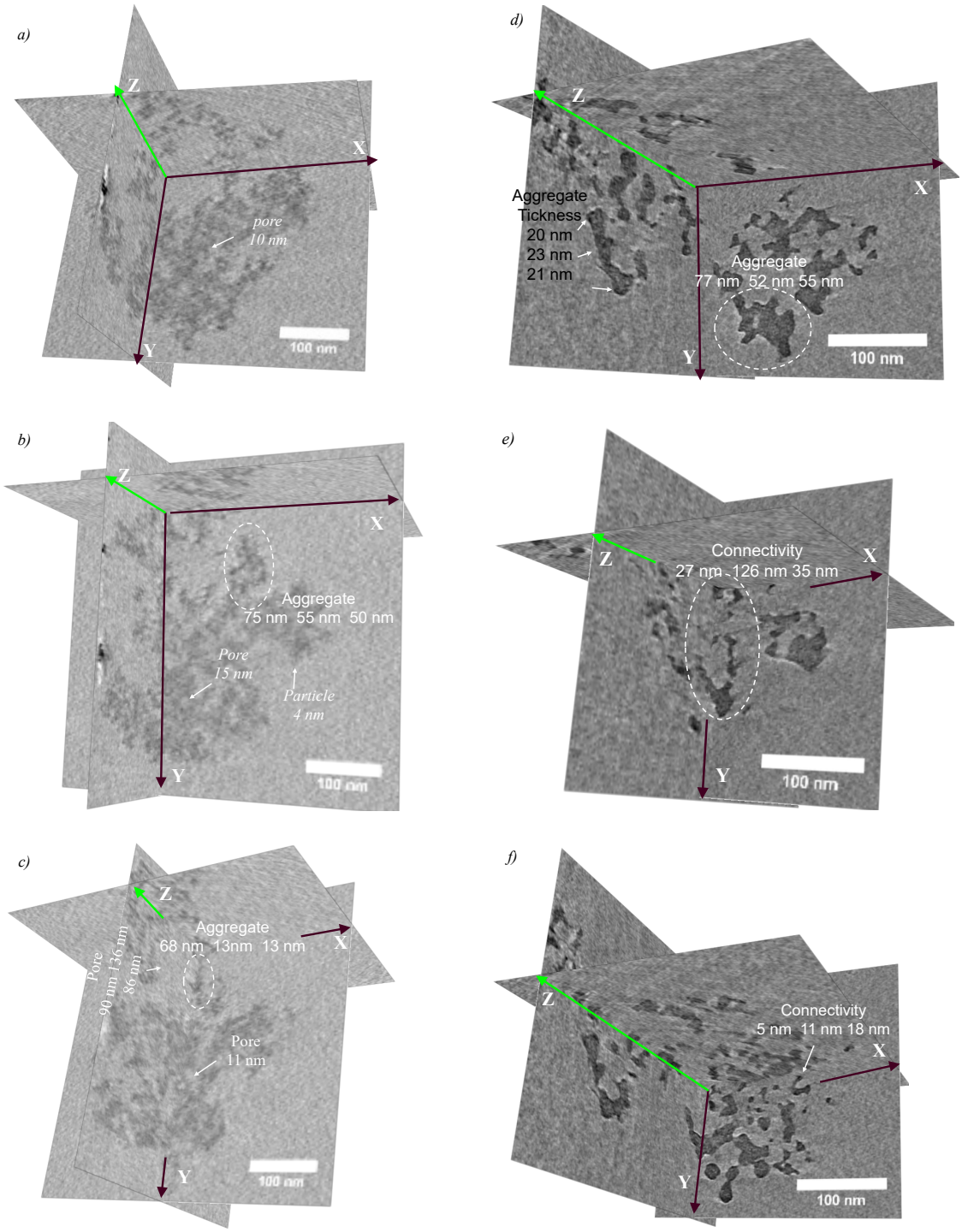

Fig SI7: Orthogonal cross-sections of the reconstructed volumes obtained using 3D Slicer. a) b) and c) Non-aged silica, d), e) and f) Silica aged for 96 days at 70 °C under 90%RH. The orthogonal cross-sections are extracted from 3 different locations within the volumes of both samples. The scale bar is added on the XY cross-section. In the non-aged sample, because the silica particles are small and are loosely connected, the contrast between silica particles and vacuum is low. However, small pores are clearly visible. Some morphological features are indicated, such as pore diameters, connections between aggregates and aggregates sizes. It can be seen that the aged sample is formed by more compact aggregates. The measurements are performed by going through the volumes along the three directions, therefore they correspond to the real sizes of the morphological features. The ellipses are only indicating the feature measured, and are not giving their sizes.

Incoherent scattering during SANS experiments

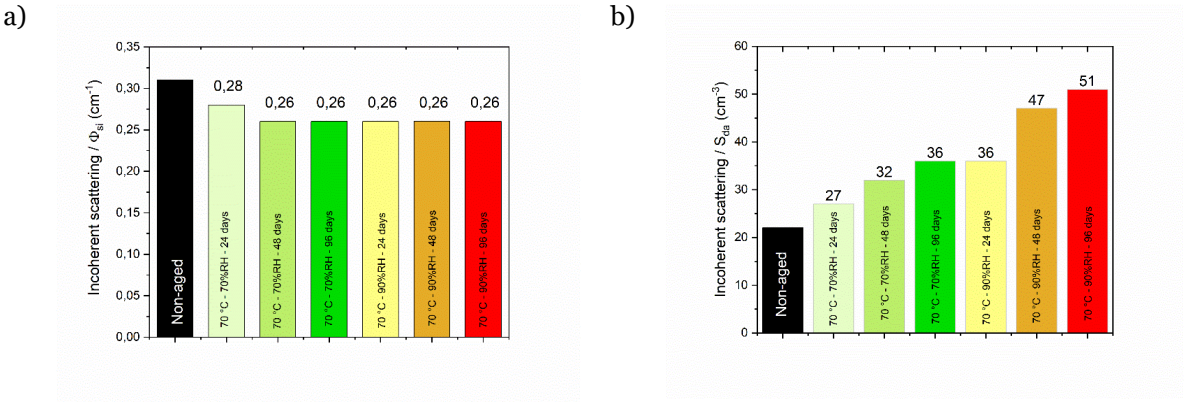

Fig SI8: Incoherent scattering background for various ageing conditions. a) The signal is normalized by the volume fraction in silica. b) the signal is normalized by the total air-silica surface area.

With the knowledge of the beam size, S_b [m²], the mass and the macroscopic surface of the pellet, m_p [g] and S_p [m²], and the specific surface area, SSA [m².g^{-1}], it is possible to determine the developed surface (*i.e.* the total surface area of the air-silica interface) which was analyzed, S_{da} [m²]:

$$S_{da} = \frac{S_b SSA m_p}{S_p}$$

Interpreting incoherent scattering first necessitates to normalize the obtain value by a volume or a surface, so that it becomes possible to compare different samples. Here, we propose two analyses of the incoherent background, by normalizing either by the silica volume fraction or by the developed surface area (see Fig. SI8).

The incoherent signal is due to the presence of hydrogen atoms. In silica, these atoms are mainly located onto the surface, as external silanol groups, Si-OH. The lowering of the incoherent background divided by the silica volume fraction along with ageing could be interpreted as a lowering of the quantity of hydrogen atoms in a given volume. This is, for example, consistent if two silanol functions react at the silica surface to give a siloxane bridge, Si-O-Si, with a molecule of water as end product. However, a part of the incoherent background also comes from physisorbed water and thus depends on the hydrophilicity at the silica surface, which also evolves during ageing.

The fact that the incoherent signal contribution normalized by the developed surface area increases with ageing can be interpreted as an increase of hydrophilicity and/or indicates a larger presence of silanol groups at the silica surface due to the ageing treatment. However, a higher proportion of silanol groups could be found “inside” the volume after ageing. For example, closed pores were highlighted by electron tomography regarding the aged silica sample. This type of tiny pores is not measured during the SSA determination by BET from N_2 sorption. In the same way, the structural reorganization occurring along with ageing could result in a less organized Si-O-Si network, with a higher proportion of silica atoms in Q_3 configuration (Si linked to three bridging oxygen atoms) with respect to Q_4 (Si linked to four bridging oxygen atoms), *i.e* more internal silanols. In this case, a part of the incoherent signal would be

inappropriately associated to an external surface, contributing to an increase of the apparent H concentration, without necessarily indicating more OH groups at the silica surface. Especially, sorption measurements (H_2O and N_2) performed on the same silica tend to show that surface hydrophilicity is relatively constant along with ageing [2].

For all the reasons cited above and given the possible superposition of several mechanisms, we think that it is difficult to draw strong conclusions from the analysis of the incoherent background. This would indeed deserve a more systematic investigation.

Mercury porosimetry

a)

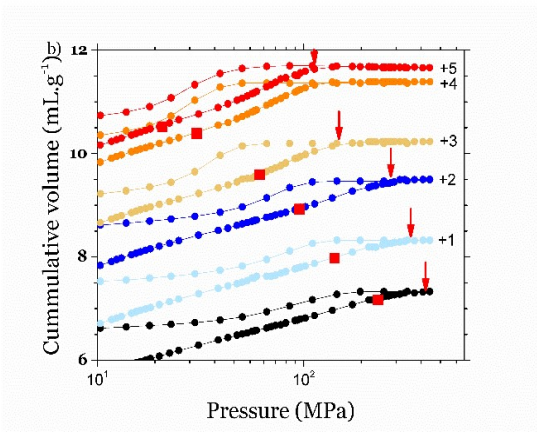

b)

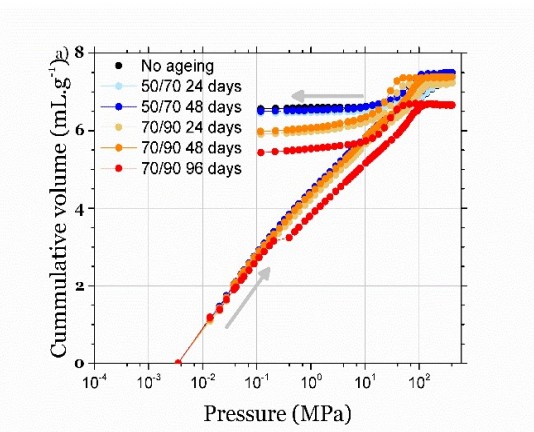

c)

Sample	Non-aged	50°C/ 70%RH 24 days	50°C/ 70%RH 48 days	70°C/ 70%RH 24 days	70°C/ 70%RH 48 days	70°C/ 90%RH 24 days	70°C/ 90%RH 48 days	70°C/ 90%RH 96 days
Inflection point [MPa]	/	207	113	66	66	56	39	38
Bulk density (3.5 kPa) [g.cm^{-3}]	0.122	0.121	0.119	0.121	0.116	0.123	0.121	0.124
η, porosity [%]	93.9	93.9	94.0	94.0	94.0	94.2	93.8	93.8
Smallest pore diameter ($2r_p$) [nm]	< 4.0	4.0	4.0	5.2	5.2	8.8	10.4	10.9

Fig SI9: Mercury porosimetry on divided powder as a function of ageing. a) and b) give the cumulative volume as the function of the pressure. Quantitative data extracted from the curves are given in c). The inflection point, frontier between the buckling domain and the Washburn domain is marked with a red square in a), and moves toward lower pressures as ageing occurs. Each red arrow in a) indicates the end of the intrusion stage in the pore network, *i.e.* the beginning of a plateau. This provides the pressure limit and thus the smallest pore size intruded. The size of the smallest intruded pore increase with ageing, as well as the overall volume of mercury retrieved and the anisotropy of intrusion/extrusion, see b). This indicate a coarsening of the pore size and an increase anisotropy in the pore network. For more clarity, not all the curves are displayed in a) and b). All quantitative data are available in c).

Supplementary Notes

Details on SANS

The radius of the elementary particle R_p [nm] was calculated from Porod's regime using the following relation:

$$R_p = \frac{6\pi\Phi_{si}\Delta\rho^2}{A}$$

Where Φ_{si} is the volume fraction of silica in the sample, $\Delta\rho^2$ is the SANS contrast between silica and air [cm^{-4}] and A is a prefactor [$cm^{-4}.nm^{-1}$].
A was experimentally extracted from the data with absolute intensities.
The contrast between silica and air was expressed from the neutron scattering length densities of both material:

$$\Delta\rho^2 = (\rho_1 - \rho_2)^2$$

The scattering length density of a molecule was estimated from the scattering length b [cm^1] of its atoms and its molecular volume ν [cm^3] according to:

$$\rho_1 = \frac{\Sigma N_i b_i}{\nu}$$

Where N_i is the number of i atoms in the considered molecule (1 for Si and 2 for O in the case of SiO_2) and b_i was taken as:

Atom	Neutron scattering length, b [cm]
Si	$4.15\ 10^{-13}$
O	$5.81\ 10^{-13}$
N	$9.36\ 10^{-13}$

We performed these calculations regarding SiO_2 and air (considering N_2 and O_2)

Molecule	Volumic mass [$g.cm^{-3}$]	Neutron scattering length density, ρ [cm^{-2}]
Air	$1.23\ 10^{-3}$	$0.00448\ 10^{10}$
SiO_2	2.0	$3.17\ 10^{10}$

It can be noticed that the neutron scattering length density of air is negligible with respect to that of silica. We finally determined that the SANS contrast between silica and air was $1.00\ 10^{21}$ cm^{-4}.

Details on mercury porosimetry experiments

Washburn's equation[3,4] is given below:

$$P_{Hg} = -\frac{2\gamma cos\theta}{r_p}$$

Where P_{Hg} is the pressure applied by mercury [Pa], r_p is the radius of the pore, γ is the surface tension (0.484-0.485 $N.m^{-1}$ at 25°C [5,6]) and θ is the angle of contact between the mercury and the material (140-141° [6]).
The porosity, η, was determined using the experimental bulk density at 3.5 kPa, ρ_{bulk} [$g.cm^{-3}$], and the skeletal density, ρ_s [$g.cm^{-3}$], as given by the supplier (2 $g.cm^{-3}$):

$$\eta = 1 - \frac{\rho_{bulk}}{\rho_s}$$

The skeletal density that mercury experiments provide as a systematic measurement skip pores lower than 3 nm and is thus an intermediate measurement. Based on this value, a fractile of measured pores is sometimes given.

Details on Nitrogen sorption

Nitrogen sorption measurements were performed on a Bel Sorp Max apparatus from Bel Japan Inc. A pre-treatment of 2 hours at 140°C under vacuum (10 Pa) was applied on 40-100 mg of material. The acquisition was done at 77.4 K. Points were acquired during sorption and desorption with partial vapor pressure from 0 to 0.997 p_0, where p_0 is the equilibrium vapor pressure of nitrogen at 77.4 K. The condition to go from one point to the next was that the pressure did not vary more than 0.3% in a 300 seconds window. The specific surface area was extracted from the BET method[7] (with an adsorption cross-section of 0.162 nm^2).

Supplementary References

1 S. Koneti, L. Roiban, F. Dalmas, C. Langlois, A. S. Gay, A. Cabiac, T. Grenier, H. Banjak, V. Maxim and T. Epicier, *Mater. Charact.*, 2019, **151**, 480–495.

2 B. Chal, B. Yrieix, L. Roiban, K. Masenelli-Varlot, J.-M. Chenal and G. Foray, *Energy Build.*, 2019, **183**, 626–638.

3 E. W. Washburn, *Proc. Natl. Acad. Sci. U. S. A.*, 1921, **7**, 115–116.

4 C. Alié, R. Pirard and J. P. Pirard, *J. Non. Cryst. Solids*, 2001, **292**, 138–149.

5 J. Rouquerol, G. Baron, R. Denoyel, H. Giesche, J. Groen, P. Klobes, P. Levitz, A. V. Neimark, S. Rigby, R. Skudas, K. Sing, M. Thommes and K. Unger, *Pure Appl. Chem.*, 2012, **84**, 107–136.

6 C. Alié, R. Pirard and J. P. Pirard, *Colloids Surfaces A Physicochem. Eng. Asp.*, 2001, **187–188**, 367–374.

7 S. Brunauer, P. H. Emmett and E. Teller, *J. Am. Chem. Soc.*, 1938, **60**, 309–319.